

EXPERIMENTAL STUDY OF AN UNSTEADY FLOWFIELD IN WING WAKE / SHOCK INTERACTIONS

Andrey M. Shevchenko Andrey S. Shmakov and Valery I. Zapryagaev

*Khristianovich Institute of Theoretical and Applied Mechanics (ITAM)
630090 Novosibirsk, Russia*

Email: shevch@itam.nsc.ru, zapr@itam.nsc.ru, web page: <http://www.itam.nsc.ru>

Key words: vortex wake, wing wake / shock interaction, pressure fluctuations, unsteady flowfield.

Abstract. A review of a comprehensive experimental study of an unsteady flowfield at different types of interactions of a wing wake with a shock wave is presented. The complex of experimental techniques included a shadowgraph visualization, and pressure fluctuations measurements. Following main topics are discussed: the interaction of a vortex wake with the bow shock generated by the cylinder obstacle; the hypersonic interaction of the vortex wake with a Pitot-type inlet.

1. INTRODUCTION

It is well known¹, that the interaction of wake vortices with the shock wave at the inlet entrance could be responsible for a reduced performance of the intake. Therefore this type of interactions was a subject for many studies. The pioneering work¹ reveals the interaction between a free vortex filament and the shock system, which exists in an intake of a supersonic aircraft. Subsequently, studies in this field were performed in Russia, France, Germany, and USA²⁻⁸. A detailed overview of numerical and experimental investigations of supersonic vortex breakdown for oblique and normal shock-vortex interaction was published by Kalkhoran and Smart⁷. One of the basic features of the vortex-shock interaction is its severe unsteadiness. It is experimentally observed in fluctuations of gas-dynamic parameters of the flow and changes in the flow structure and the size of the interaction region. Experimental data with quantitative estimates of manifestations of unsteadiness are rather limited. The absence of numerical and experimental data for hypersonic velocities should be specially noted. Obtaining results for this range of velocities is extremely important for the development of promising flying vehicles (avoiding of catastrophic operation regimes of a hypersonic inlet and improvement of mixing in the combustor).

Recently a hypersonic interaction of a wing-tip vortex with a Pitot type inlet has been examined at Mach number of $6^{9,10}$. Initially these experiments were performed to extend the experimental data⁵ to a hypersonic Mach numbers range. It was obtained that the wing-tip vortex is the initiator of self-oscillatory process with salient fundamental. Fundamental frequency as well as static pressure distribution along the inlet slightly

depends on the vortex strength⁹. Borovoy et al⁸ revealed a strong influence of a vortex on heat transfer on a blunted body.

Therefore two sets of experiments were performed. The first one was directed to conduct an experimental study simulating the interaction of a Pitot type inlet with wakes generated by a wing and a body of revolution. The main goal of these experiments was to reveal the similar properties and differences in interaction of a wake and a vortex with a Pitot type inlet. An investigation of an unsteady nature of a wing wake / bow shock wave interaction in a wide Mach number range of 3 - 6 is aim of the second set of the experiments.

2. WAKE / PITOT TYPE INLET INTERACTION

2.1. Experimental setup and techniques

Experiments were conducted in the hypersonic wind tunnel T-326 of the Khristianovich Institute of Theoretical and Applied Mechanics of the Russian Academy of Sciences. It is an intermittent blowdown facility with the gas flow through a nozzle into the Eiffel chamber. The wind tunnel is capable of producing a Mach number range from 6 to 14. The Pitot-type inlet is the tube with sharp leading edge and the diameter of 30 mm and the length of 70 mm. A normal shock wave is created in front of the inlet by an adjustable obstruction in the form of truncated cone. Two different test models were

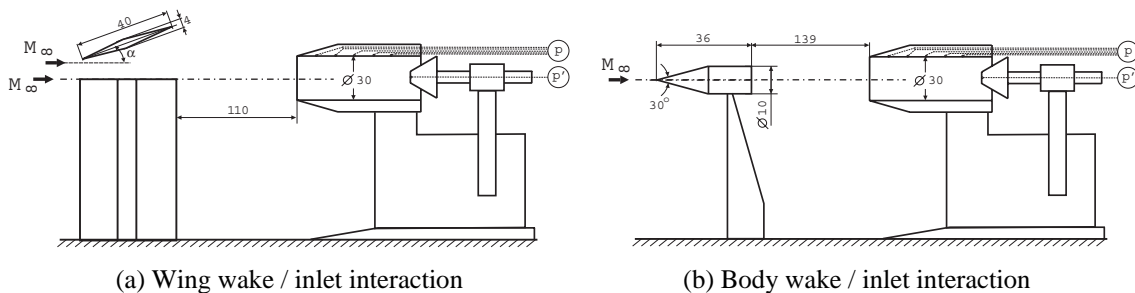
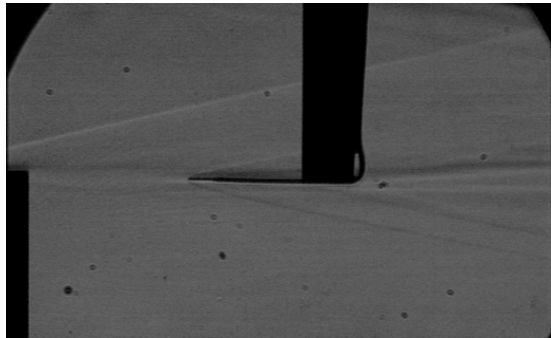


Figure 1. Sketch of experiments (not to scale)

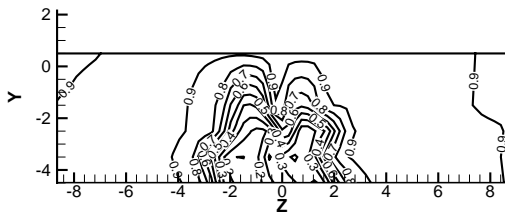
used to generate a vortical flowfield in front of the inlet (Fig. 1). The first one is the vortex generator which represents a rectangular half-wing with a span of 200 mm. A hexahedral airfoil has a chord length of 40 mm and thickness of 4 mm. The wing was mounted on the Eiffel chamber floor at the nozzle centerline (Fig. 1a). The vortex generator could be set at different angles of attack in the range from -30 deg to 30 deg. The second set of experiments was created to study the flowfield behind of a body of revolution (see Fig. 1b). The test model was a "sharp cone-cylinder" combination with total length of 36 mm and diameter of 10 mm. The forebody aspect ratio was 1.8. The model was mounted in the Eiffel chamber at zero angle of incidence. In the first set of experiments the Pitot-type inlet was mounted 110 mm downstream from the trailing edge of the rectangular wing. In the second set the inlet was placed 139 mm downstream from the rear of the body. In preliminary experiments the Pitot probe with an outer diameter of 0.8 mm was used to obtain Pitot pressure data upstream of the inlet. The shadowgraph visualization of the flowfield was carried out using a spark light source with 3 microsecond exposure times. Shadowgraph images were recorded at a rate of 33 frames per second. Piezoelectric fast-response pressure transducer was used to measure of pressure pulsation on the butt of the cone obstruction (Fig. 1). The

amplified output from the transducer was digitized using an AD converter at a rate of 100 kHz. Time-averaged static pressure distribution along of the inlet was measured as well. Experimental equipment and flow visualization system allows obtain shadowgraphs and simultaneously record the pressure pulsation data. The experiments were performed at Mach number of 6 and corresponding unit Reynolds number of 11 million per meter. Experimental data were obtained for wing angles of attack up to 15 deg with the step of 2.5 deg.

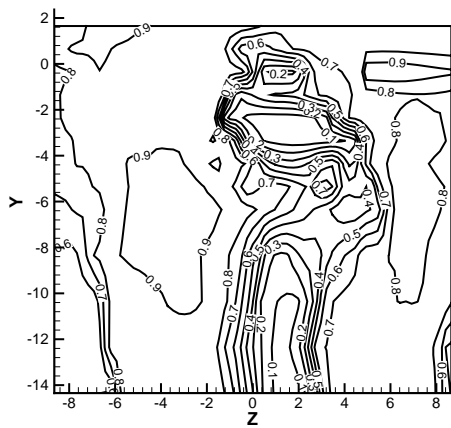
2.2. Results and discussion



(a) Shadowgraph at $\alpha=10$ deg

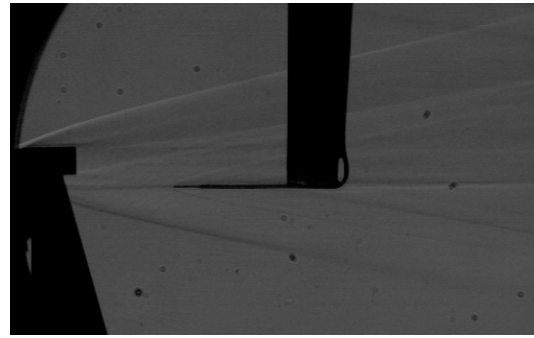


(b) Pitot pressure contours at $\alpha=0$

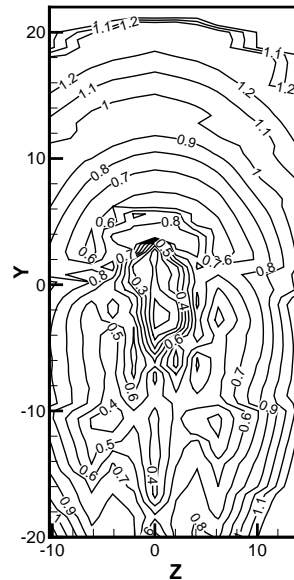


(c) Pitot pressure contours at $\alpha=10$ deg

Figure 2. The flowfield behind of the wing



(a) Shadowgraph



(b) Pitot pressure contours $\alpha=10$ deg

Figure 3. The flowfield behind of the body

Figures 2a and 3a show typical shadowgraphs during Pitot pressure measurements in wakes behind of a rectangular wing and a body of revolution. The probe size was rather small in order to decay the flowfield structure.

Fig. 2b illustrates upper part of Pitot pressure contours for the wing wake at zero angle of attack. As shown the contours are approximately symmetrical and typical for the

wake without a vortex. Figure 2c shows Pitot pressure contours in a wake behind of a rectangular wing at angle of attack $\alpha=10$ deg in a cross-section 55 mm downstream from trailing edge of vortex generator. A comparison of the visualization and pressure probe measurements results showed that flows in a wakes behind of a rectangular wing and a body of revolution are characterized by a decrease in total pressure. There are two areas of Pitot pressure deficit can be observed. The top closed contours correspond to the vortex core and lower zone of Pitot pressure loss corresponds to the wing wake. Figure 3b shows Pitot pressure contours in a wake behind of the body. The data were obtained in the cross-section located 35 mm downstream from the rear of the body. The top region with approximately circular contours corresponds to the wake behind the body. At the lower part Pitot pressure contours are deformed due to the influence of the supporting pylon. It should be noted that Pitot pressure loss in the wing wake is greater then in the case of the wake after the body of revolution. The results obtained serve as initial data for experimental investigation of interaction of a Pitot-type inlet with near wake behind of a rectangular wing and a body of revolution.

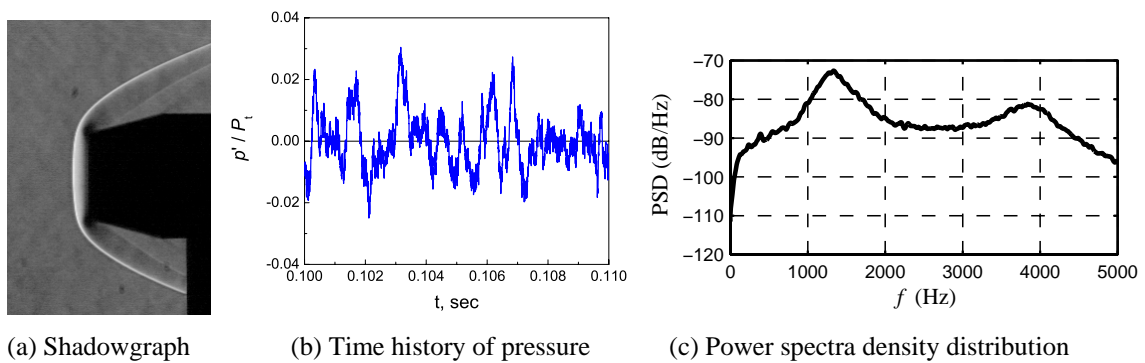


Figure 4. Pitot-type inlet in free stream

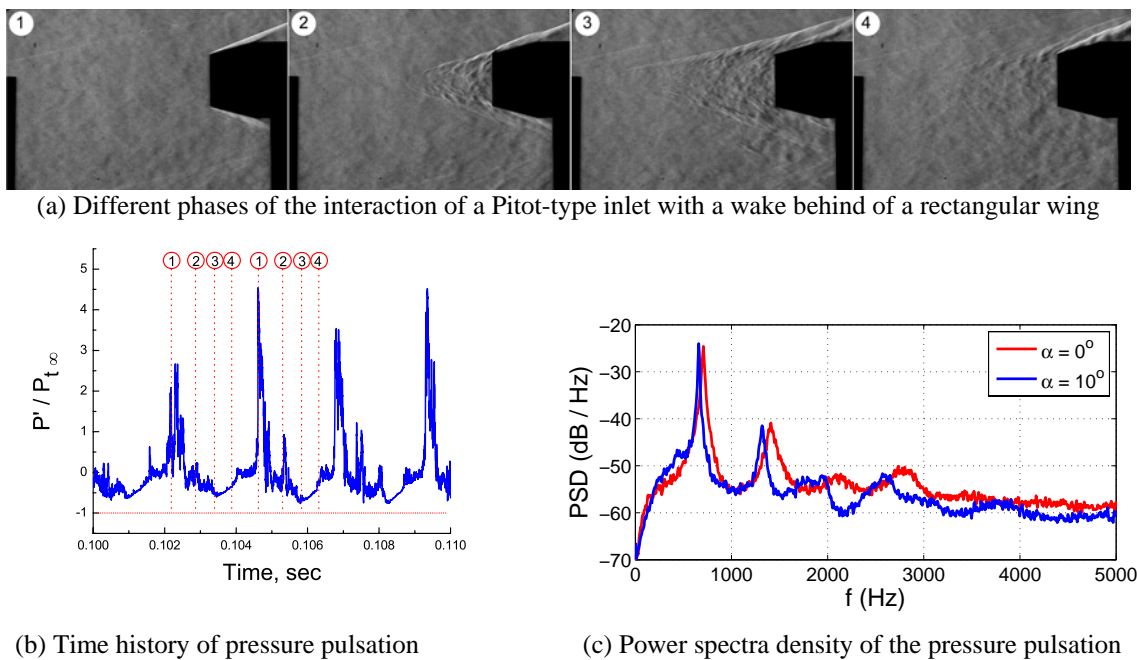
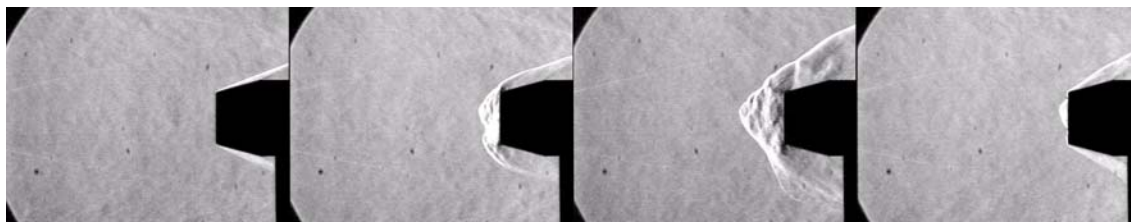


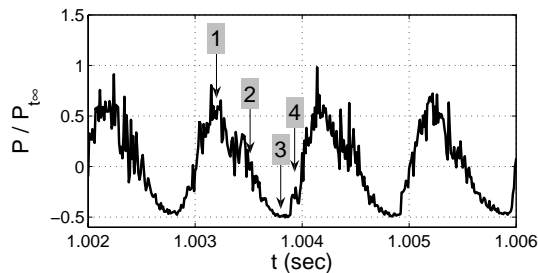
Figure 5. Experimental data of the interaction of a Pitot-type inlet with a wake behind of a rectangular wing (angle of attack $\alpha=10$ deg)

Fig. 4 shows experimental results for the inlet in free stream. At the inlet axis the bow shock is approximately normal (Fig. 4a). The magnitude of pressure pulsation doesn't exceed of 3% of mean Pitot pressure (Fig. 4b). Examination of the power spectral density indicated a fundamental with a sufficiently low power and a frequency of about 1330 Hz associated with a quarter-wave resonance (Fig. 4c).

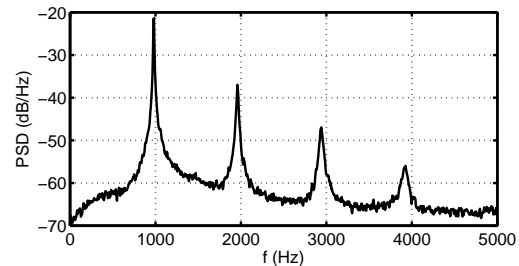
Figure 5 shows typical shadowgraphs and the pressure fluctuations data during wing wake / inlet interaction. The following phases of the self-oscillatory process can be distinguished. The first phase corresponds to upstream motion of the compression wave inside the Pitot-type inlet from the throttling device. The beginning of this phase displays the maximum values of pressure which several times exceed free stream Pitot pressure. The second phase corresponds to upstream motion of the shock wave from the leading edge of the Pitot-type inlet to the wing. A region of an intensely vortical flow is seen behind the wave front. This phase involves a certain decrease in pressure at the end face of the throttling device. When the shock wave reaches the wing the minimum of pressure is fixed. Then there is a destruction of a shock wave and movement of a vortical flow to the channel. In this phase, an increase in pressure at the end face of the throttle is registered. The spectral analysis performed has clearly expressed discrete components of the pressure fluctuation signal (Fig. 5c). Similar results were obtained for all cases of wing wake / inlet interaction ($\alpha=0-15$ deg).



(a) Different phases of the body wake / Pitot-type inlet interaction



(b) Time history of pressure pulsation



(c) Power spectra density of the pressure pulsation

Figure 6. Body wake / Pitot-type inlet interaction

Figure 6 shows typical shadowgraphs and the pressure fluctuations data for the interaction of the Pitot-type inlet with a wake behind of the body of revolution. As well as for the case of wing wake / inlet interaction a high unsteady process has revealed for the body wake / inlet flowfield. But some essential differences can be detected. First, the level of pulsations is a little bit less, and, second, the length of the interaction region is much shorter. It has not been fixed any case when the interaction region reached up to the body.

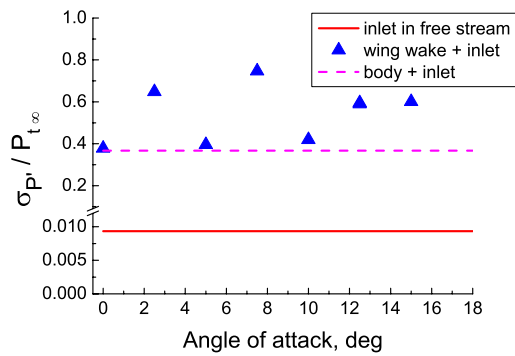


Figure 7. Standard deviation vs α

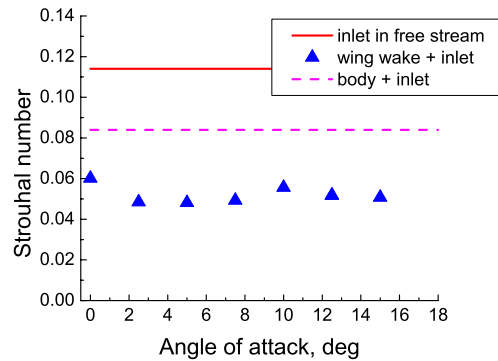


Figure 8. Strouhal number vs α

Figures 7 and 8 show plots of standard deviation of pressure fluctuations and Strouhal number versus an angle of attack of the wing respectively. Strouhal number was defined on a fundamental frequency. It is seen, that there is no monotonous dependence of the specified values on an angle of attack. Strouhal number for wing wake / inlet interaction is approximately two times less than Strouhal number, associated with the inlet in free stream (Fig. 8). On the other hand, the standard deviation of pressure for the case of wing / Pitot-type inlet interaction are two orders greater than one obtained for the inlet in free stream (Fig. 7). The fundamental frequency for the body / inlet interaction is much more than the frequency corresponding to the wing / inlet interaction and sufficiently less than the frequency for the inlet in the free stream. For both cases of the interactions standard deviations are received of the same order. Figure 9 shows static pressure distribution along the inlet.

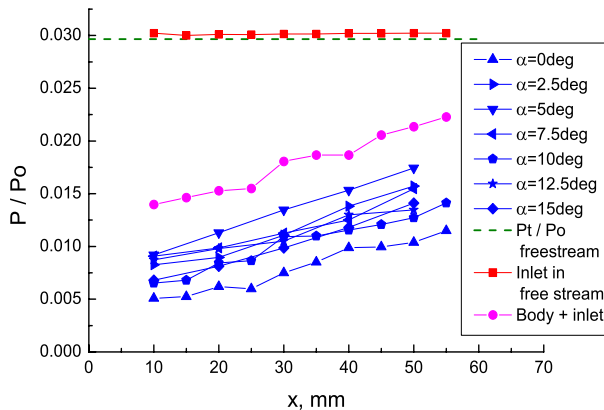


Figure 9. Time-averaged pressure distribution along the inlet.

pressure distribution along the inlet. As one would expect, in the case vortex / inlet interaction the pressure decrease in comparison with the case of the inlet without the interaction. But it's impossible to specify the certain dependence of the pressure distribution on an angle of attack of the wing. In the case body / inlet interaction the pressure still decreases in comparison with inlet in free stream, but increases in comparison with the case vortex / inlet interaction.

Thus the wake behind of a body of revolution as well as the wake behind a rectangular wing is the initiator of self-oscillatory process with silent fundamental. The fundamental frequency as well as a static pressure distribution along the inlet for the case body / inlet interaction is slightly greater than for the case of vortex / inlet interaction. Apparently the self-oscillatory process is caused by non-uniformity of a Mach number and total pressure at the inlet entrance. Therefore the experiments on a vortex / Pitot type inlet interaction do not simulate the nature of a vortex / normal shock wave interaction. It is another problem studying an interaction of a vortex wake with the channel.

3. WING WAKE / BOW SHOCK WAVE INTERACTION

3.1. Experimental setup and techniques

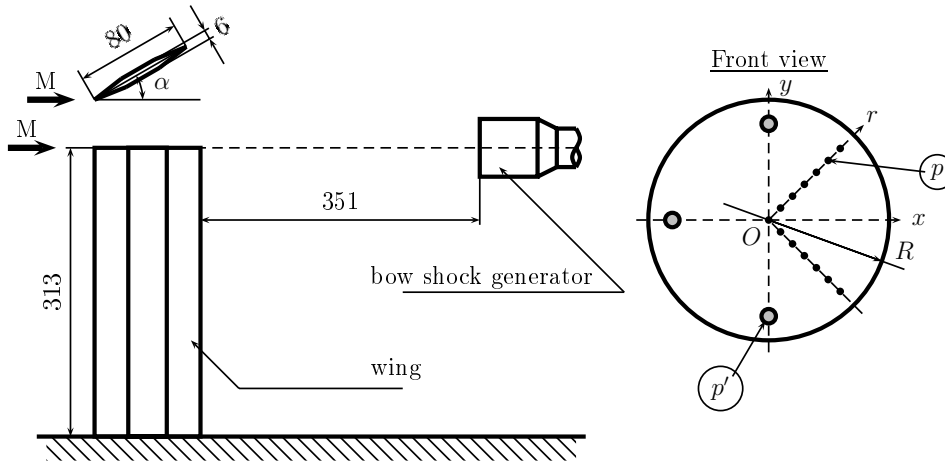


Figure 10. Schematic of the experimental setup (not to scale, all dimensions are in mm)

The experimental study of the interaction of a vortex wake with a bow shock wave were carried out in the supersonic blow-down wind tunnel T-313 of the Khristianovich Institute of Theoretical and Applied Mechanics of the Russian Academy of Sciences. It is an intermittent blowdown facility with the test section dimensions of $0.6 \times 0.6 \times 2$ m. The wind tunnel is capable of producing a Mach number range from 1.75 to 7 and unit Reynolds numbers in the range of $(10 - 80) \cdot 10^6$ per meter.

Figure 10 illustrates the schematic representation of the experimental setup. A wing-tip vortex is generated by an unswept semispan slender wing. A hexahedral airfoil has a chord length of 80 mm, a half-angle of 8 deg. The wing was mounted on the test section floor at the tunnel centerline. The vortex generator could be set at different angles of attack in the range from -30 to 30 deg. The bow shock wave is generated by a cylinder obstacle with a radius $R = 100$ mm. The cylinder is placed 351 mm downstream of the trailing edge of the wing.

Shadowgraphs of the flow were taken using a novel visualization technique¹¹. Instead of Foucault knife we used a plate made of phototropic glass, further - AVT (adaptive visualizing transparency). Under the influence of focused radiation the AVT material darkens pro rata to intensity. The sensing radiation which is being deflected even at small disturbances on very small angles goes through non-black-out area of AVT and reveals in the shadow picture as more bright part. The great advantage of this technique is an opportunity to visualize weaker perturbations against a background of stronger ones. The scheme as being self-adjusting one essentially simplifies the process of the experiment. The shadowgraph images were carried out using a spark light source with 2.5 microsecond exposure times. The images were recorded at a rate of 8 frames per second. Three piezoelectric fast-response pressure transducer were used to measure of pressure pulsation on the face of the cylinder. The transducers were placed on distance $0.75R$ from the center of the cylinder (Fig. 10). The amplified output from the transducer was digitized using an AD converter at a rate of 100 kHz. Time-averaged pressure distribution on the cylinder butt was measured as well. The pressure ports were located along a line marked as r in 8.

At $M = 6$ experimental data were obtained for wing angles of attack up to 20 deg with the step of 5 deg. At $M = 3$ and 4 the experiments were performed for wing angles of attack up to 10 deg with the step of 2.5 deg.

3.2. Flowfield in a wake behind of the wing

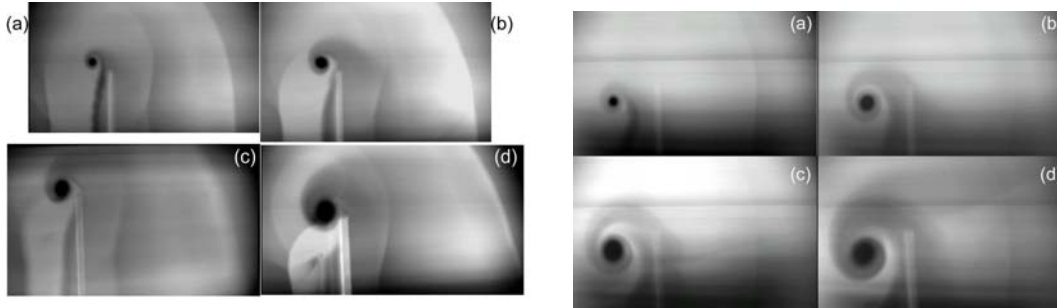


Figure 11. Laser sheet images for $x/b=1.5$ (left) and $x/b=3.0$ (right):
(a) $\alpha=5$ deg; (b) $\alpha=10$ deg; (c) $\alpha=15$ deg; (d) $\alpha=20$ deg.

In preliminary experiments a flowfield behind of the wing was examined with a laser sheet imaging technique and multi-hole pressure probe technique⁹. Three 5-hole conical pressure probes were used to measure local Mach number, Pitot pressure and flow angularity in the core of the wing-tip vortex and its vicinity. Each probe has an outer diameter of 3 mm. Quantitative flowfield measurements and laser sheet visualization were performed at two cross-sections at the distance of 120 mm and 240 mm downstream from the wing trailing edge. The experiments were performed at Mach numbers of 3 and 4, and corresponding unit Reynolds numbers of 36 and 56 million per meter. Vortex generator was mounted at angles of attack $\alpha = 5, 10, 15$ and 20 deg.

Figure 10 shows typical images obtained with the laser sheet technique. In these figures, the vortex core is seen as a black region. In the near wake ($x/b=1.5$) the laser sheet images has revealed a complicated flowfield structure with formations of the bow shock, inner shocks and expansion waves. The observed flowfield is similar to the flow topology over a rectangular wing⁸. In the far wake ($x/b=3$) only the bow shock and the vortex sheet which roll-up of the vortex core are visible. Inner shocks and expansion waves are dissipated. In these figures, the vortex core is seen as a black region.

Figure 12 show typical results of 5-hole pressure probe measurements. These measurements yielded detailed data on the fields of total pressure, Mach number, and Mach number components onto the axes of the flow-fitted coordinate system. As is well known in the vortex core the radial component of velocity is small as compared with the circumferential velocity. Thus it is easy to show that crossflow Mach number defined as $M_{zy} = \sqrt{M_z^2 + M_y^2}$ is a good estimate of circumferential Mach number and $\tau = M_{zy} / M_x$ is estimation of swirl ratio. A comparison of visualization and probe measurements results showed that the vortex core, which looks as a dark region in the laser sheet images, is characterized by a decrease in total pressure, Mach number, and axial component of velocity; thus, a wake-type profile is formed. The maximum values of the circumferential velocity as well as swirl ratio correspond to the edge of the vortex-core (Fig. 12d).

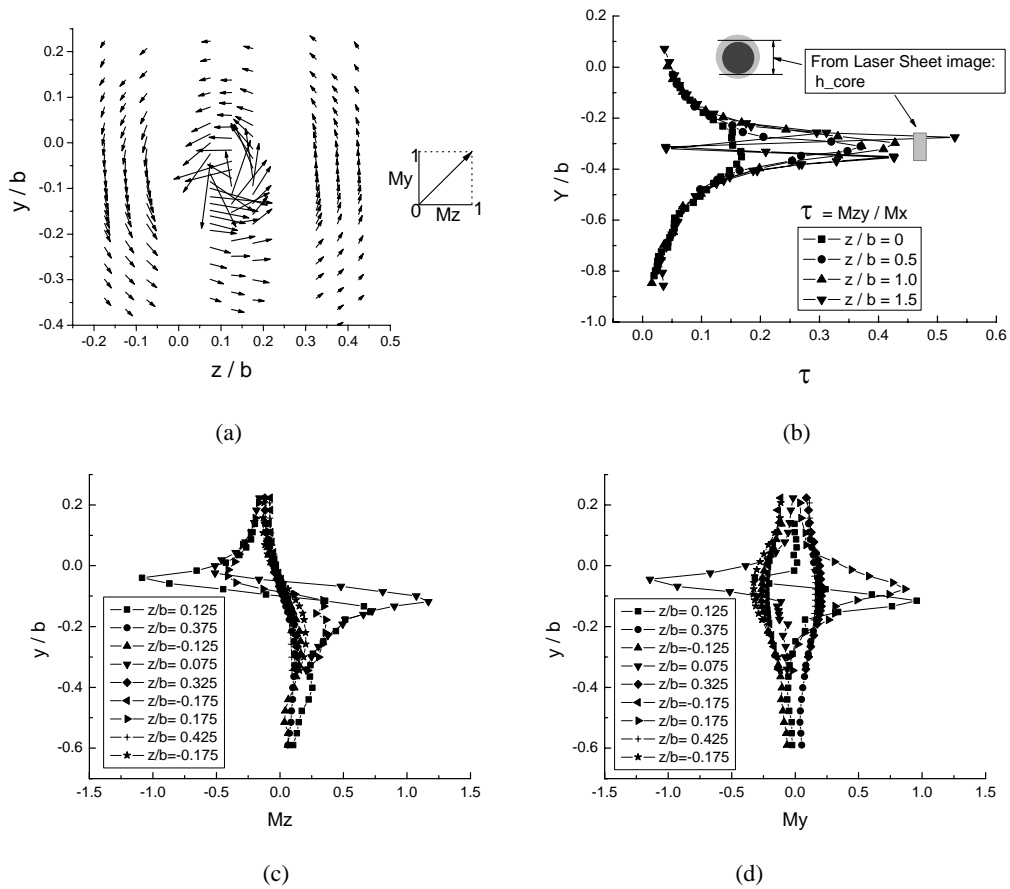


Figure 12. Five-hole pressure probe data through the vortex core for $M=4$, $\alpha=10$ deg: (a) crossflow vectors; (b) swirl ratio; (c) horizontal Mach number; (d) vertical Mach number.

This experiments revealed many vortex core characteristics commonly found in previous studies of supersonic wing-tip vortices¹² and leading-edge vortices¹³, including an asymmetric swirl distribution and significant total pressure and total Mach number deficits. The spatial scale, Mach number deficit and total pressure loss of the vortices were observed to increase with wing angle of attack.

3.3. The interaction at Mach numbers of 3 and 4

In experiments without the wing a well known flowfield with a detached bow shock was observed. The flowfield is steady without of any noticeable variation of the distance between the bow shock and the cylinder face. Time-averaged pressure distribution is typical (see Fig. 14). The standard deviation of pressure fluctuations did not exceed of 1% of mean free-stream Pitot pressure. Figure 13 shows typical shadowgraphs of the flowfield generated during the interaction at $M = 4$. At $\alpha = 0$ and 2.5 deg the interaction zone represents complex pulsing unsteady region. The shape of the bow shock wave and the size of the interaction region change during one test (Fig. 13b). Figure 14 shows time-averaged pressure distribution on the cylinder butt. It displays that the pressure decreases in the central part of the cylinder while the angle of attack increases up to 5 deg.

At $\alpha = 5$ deg the flow field is similar that one observed in previous study of the normal shock/vortex interaction^{6,8,9} (see Fig. 13c and 13d). In this case the interaction region is bounded by a round-nosed conical shock wave. The interaction region consists of two zones: a central zone containing the distorted vortex and an outer supersonic zone

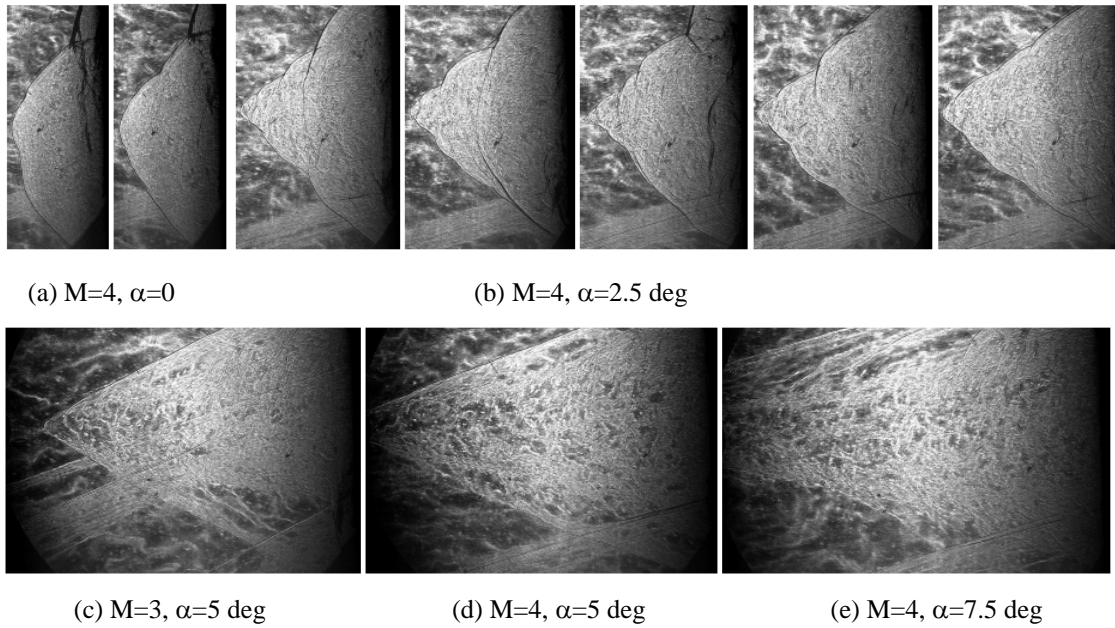


Figure 13. Shadowgraphs of the flow during bow shock / vortex interaction

bounded by the conical bow shock wave. The weak waves in this (outer) zone may be visible in Fig. 13. At $\alpha = 7.5$ deg the interaction region extends upstream from the cylinder right up to the wing (Fig. 13e). For $\alpha = 5$ and 7.5 deg an examination of multiple spark shadowgraphs has revealed an unsteady character of the interaction. But in contrast to the case $\alpha = 2.5$ deg the shape of the conical shock does not change.

It is seen from Fig. 14, that at $\alpha > 5$ deg the pressure distribution does not depend on the angle of attack of the wing. In the central part of the cylinder it does not exceed 25% of the Pitot pressure in free-stream. It corresponds to the results received in previous experiments and is caused, apparently Pitot pressure loss in the vortex wake behind the wing^{9,12}.

Thus, at a pulsing mode the pressure decreases with growth while the angle of attack increases. When the shape of the bounded shock does not change or the interaction region extends upstream to the wing the pressure distribution does not depend on the angle of attack. The measured pressure fluctuations at the butt of the shock-wave generator confirm the extremely unsteady character of interaction. At the same time, the spectral analysis has not revealed significant peaks in the normalized power spectral density distribution.

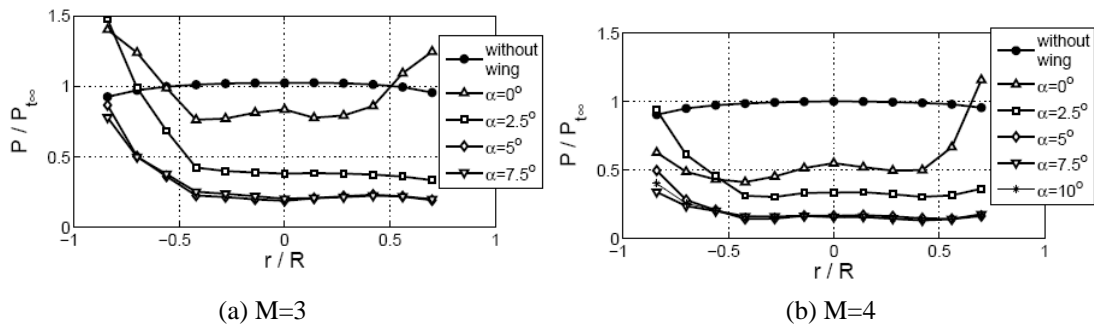
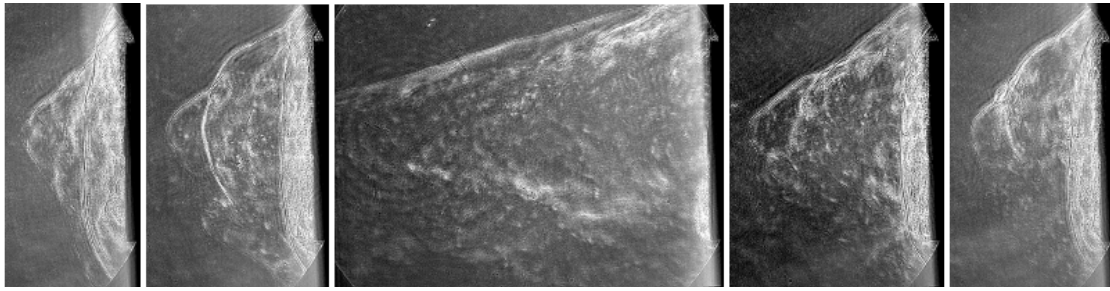
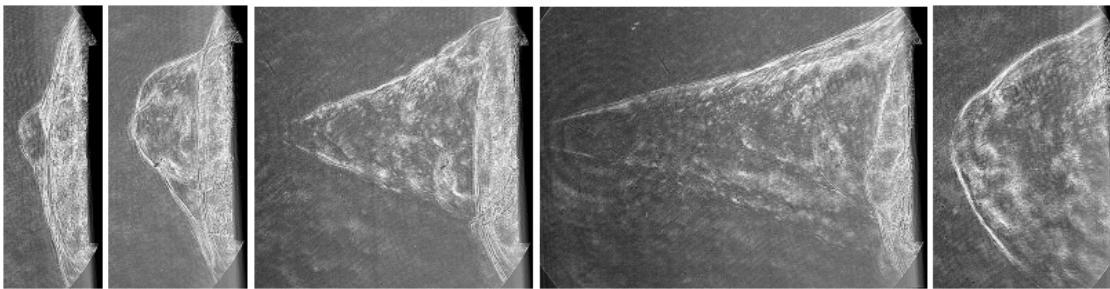


Figure 14. Time-averaged pressure distribution on the cylinder butt

3.2. The interaction at Mach number of 6



(a) $\alpha=5$ deg



(b) $\alpha=10$ deg

Figure 15. Shadowgraph at M = 6

Figure 15 illustrates typical shadowgraphs of the flowfield at the Mach number of 6. This figure clearly indicates the oscillating process during the hypersonic interaction of a wing wake with a bow shock wave. Only at a zero angle of attack the interaction region of a finite size was observed. Otherwise ($\alpha = 5\div 20$ deg) it pulsed upstream from the cylinder up to the wing.

The pressure measurements confirm the occurrence of a pulsing interaction process. The normalized power spectral density distribution displays sufficiently high power of the pressure fluctuations. Figure 16 indicates a fundamental with a sufficiently high power and a frequency of about $f = 380\text{--}450$ Hz associated with the occurrence of a self-oscillatory process during the interaction at $\alpha=10\div 20$ deg. Subharmonics also are visible in this figure. At $\alpha = 0$ and 5 deg the pressure fluctuation power is sufficiently high. But the normalized power spectral density distribution has no peaks.

Figure 17 shows a time-averaged pressure distribution at Mach number of 6. It is seen that the pressure at central part of the cylinder does not depend of an angle of attack. It

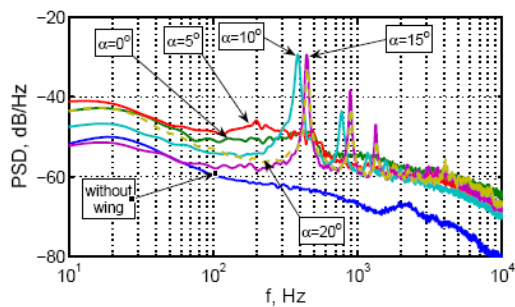


Figure 16. Power spectral density distribution

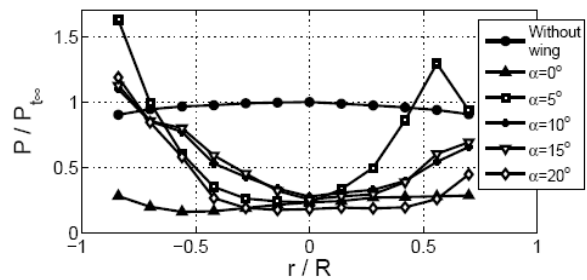


Figure 17: Time-averaged pressure distribution

corresponds to the case while the interaction region extends upstream to up to the wing.

5. CONCLUSION

An experimental study involving interaction of vortex wakes behind of a rectangular wing and a body of revolution was carried out at Mach number of 6. It was obtained that the wake behind a wing or a wake behind a body cause a self-oscillatory process with salient fundamental. Fundamental frequency as well as static pressure distribution along the inlet slightly depend on the vortex strength.

The interaction of a vortex wake with a bow shock wave was studied at a Mach numbers range from 3 to 6. The experiments revealed a highly unsteady processes during the interactions. Global reorganization of flowfield structure with a high level of pressure fluctuations was observed. At low angles of attack the experiments has detected an interaction process with a pulsing bow shock wave. The self-oscillatory process was revealed at Mach number of 6.

ACKNOWLEDGEMENTS

The work was supported by the Russian Foundation for Basic Research, grant No. 06-01-00774.

10. REFERENCES

- [1] V.V. Zatuloka, A.K. Ivanyushkin, A.V. Nikolayev, "Interference of vortices with shocks in aircoops. Dissipation of vortices", *Fluid Mechanics, Soviet Research*, Vol. 7, 153-158, (1978).
- [2] J. Delery, E. Horowitz, O. Leuchter, J. Solignac, "Fundamental Studies on Vortex Flows", *La Recherche Aerospaciale, (English ed.)*, 1-24, (1984).
- [3] G.F. Glotov, "Interference of a vortex core with shock waves in a free stream and nonisobaric jets", *Uchenie zapiski TsAGI*, Vol. 20, No. 5, (in Russian), (1989).
- [4] A.K. Ivanyushkin, Yu.V. Korotkov, A.V. Nikolayev, "Some features of an interference of shock waves with aerodynamic wake", *Uchenie zapiski TsAGI*, Vol. 20, No. 5, (in Russian) (1989).
- [5] L. Cattafesta and G. Settles, "Experiments on shock/vortex interaction", *AIAA Paper*, No 0315, (1992).
- [6] I.M. Kalkhoran, M.K. Smart, A. Betti, "Interaction of a supersonic wing tip vortex with a normal shock", *AIAA Journal*, Vol. 3, No. 34, 1855-1861, (1996).
- [7] I.M. Kalkhoran, M.K. Smart, "Aspects of shock wave-induced vortex breakdown", *Progress in Aerospace Sciences*, Vol.30, 63-95, (2000).
- [8] V.Ja. Borovoy, T.V. Kubishina, A.S. Skuratov, L.S. Yakovleva, "Vortex in a supersonic flow and its influence on a flowfield and heat transfer of the blunted body", *Mechanica zhidkosti i gaza*, No. 5, 66-76, (in Russian), (2000).

- [9] A. Shevchenko, I. Kavun, A. Pavlov, V. Zapryagaev, "Review of ITAM experiments on shock / vortex interaction", *European Conference for Aerospace Sciences*, Moscow, July 4-7, 2005, Paper No. 2.07.01., (2005).
- [10] A. Shevchenko, I. Kavun, A. Pavlov, V. Zapryagaev, "Visualization of wing-tip vortices and of an unsteady flowfield in shock / vortex interaction", *12th Intern. Symp. on Flow Visualization*, Gottingen, Germany, September 10-14, 2006, ISBN 0-9533991-8-4, Paper No. 219, (2006).
- [11] M.P. Golubev, A.A. Pavlov, Al.A. Pavlov. "Use of phototropic materials as visualizing transparency in shadow devices", *9th International Scientific and Technical Conference "Optical Methods of Flow Investigation"*, June 27-29, Moscow, (2007).
- [12] M.K. Smart, I.M. Kalkhoran, J. Bentson, "Measurements of supersonic wing tip vortices", *AIAA Journal*, Vol. 33, No. 10, 1761-1768, (1995).
- [13] M.D. Brodetsky and A.M. Shevchenko, "Experimental investigation of the supersonic flow on a lee side of a delta wing", *Thermophysics and Aeromechanics*, Vol. 5, No. 2, 307-318, (1998).